

## **Aberrant function of the C-terminal tail of HIST1H1E accelerates cellular senescence and causes premature aging**

Elisabetta Flex,<sup>1,30</sup> Simone Martinelli,<sup>1,30</sup> Anke Van Dijck,<sup>2,3,30</sup> Andrea Ciolfi,<sup>4</sup> Serena Cecchetti,<sup>5</sup> Elisa Coluzzi,<sup>6</sup> Luca Pannone,<sup>1,4</sup> Cristina Andreoli,<sup>7</sup> Francesca Clementina Radio,<sup>4</sup> Simone Pizzi,<sup>4</sup> Giovanna Carpentieri,<sup>1,4</sup> Alessandro Bruselles,<sup>1</sup> Giuseppina Catanzaro,<sup>8</sup> Lucia Pedace,<sup>9</sup> Evelina Miele,<sup>9</sup> Elena Carcarino,<sup>9</sup> Xiaoyan Ge,<sup>10,31</sup> Chieko Chijiwa,<sup>11</sup> M.E. Suzanne Lewis,<sup>11</sup> Marije Meuwissen,<sup>2</sup> Sandra Kenis,<sup>3</sup> Nathalie Van der Aa,<sup>2</sup> Austin Larson,<sup>12</sup> Kathleen Brown,<sup>12</sup> Melissa P. Wasserstein,<sup>13</sup> Brian G. Skotko,<sup>14</sup> Maria Karayiorgou,<sup>15</sup> J. Louw Roos,<sup>16</sup> Koen L. Van Gassen,<sup>17</sup> Marije Koopmans,<sup>17</sup> Emilia K. Bijlsma,<sup>18</sup> Gijs W.E. Santen,<sup>18</sup> Daniela Q.C.M. Barge-Schaapveld,<sup>18</sup> Claudia A.L. Ruivenkamp,<sup>18</sup> Mariette J.V. Hoffer,<sup>18</sup> Seema R. Lalani,<sup>10</sup> Haley Streff,<sup>10</sup> William J. Craigen,<sup>10</sup> Brett H. Graham,<sup>10,19</sup> Annette P.M. van den Elzen,<sup>20</sup> Daan J. Kamphuis,<sup>21</sup> Katrin Õunap,<sup>22</sup> Karit Reinson,<sup>22</sup> Sander Pajusalu,<sup>22,23</sup> Monica H. Wojcik,<sup>24</sup> Clara Viberti,<sup>25,26</sup> Cornelia Di Gaetano,<sup>25,26</sup> Enrico Bertini,<sup>4</sup> Simona Petrucci,<sup>27,28</sup> Alessandro De Luca,<sup>28</sup> Rossella Rota,<sup>9</sup> Elisabetta Ferretti,<sup>8,29</sup> Giuseppe Matullo,<sup>25,26</sup> Bruno Dallapiccola,<sup>4</sup> Antonella Sgura,<sup>6</sup> Magdalena Walkiewicz,<sup>10,32</sup> R. Frank Kooy,<sup>2,33,\*</sup> Marco Tartaglia,<sup>4,33,\*\*</sup>

<sup>1</sup>Department of Oncology and Molecular Medicine, Istituto Superiore di Sanità, Rome, 00161 Italy.

<sup>2</sup>Department of Medical Genetics, University of Antwerp, Edegem, 2650 Belgium.

<sup>3</sup>Department of Neurology, Antwerp University Hospital, Edegem, 2650 Belgium.

<sup>4</sup>Genetics and Rare Diseases Research Division, Ospedale Pediatrico Bambino Gesù, IRCCS, Rome, 00146 Italy.

<sup>5</sup>Microscopy Area, Core Facilities, Istituto Superiore di Sanità, Rome, 00161 Italy.

<sup>6</sup>Department of Science, University "Roma Tre", Rome, 00146 Italy.

<sup>7</sup>Department of Environment and Health, Istituto Superiore di Sanità, Rome, 00161 Italy.

<sup>8</sup>Department of Experimental Medicine, Sapienza University, Rome, 00161 Italy.

<sup>9</sup>Oncohematology Research Division, Ospedale Pediatrico Bambino Gesù, Rome, 00146 Italy.

<sup>10</sup>Department of Molecular and Human Genetics, Baylor College of Medicine, Houston, TX 77030, USA.

<sup>11</sup>Department of Medical Genetics, University of British Columbia, Vancouver, British Columbia V6H 3N1, Canada.

<sup>12</sup>Department of Pediatrics, Section of Clinical Genetics and Metabolism, University of Colorado Anschutz Medical Campus, Children's Hospital Colorado, USA.

<sup>13</sup>Children's Hospital at Montefiore, Albert Einstein College of Medicine, New York, NY 10467, USA.

<sup>14</sup>Department of Pediatrics, Massachusetts General Hospital, Department of Pediatrics, Harvard Medical School, Boston, MA 02114, USA.

<sup>15</sup>Department of Psychiatry, Columbia University Medical Center, New York, NY 10032, USA.

<sup>16</sup>Department of Psychiatry, University of Pretoria, Weskoppies Hospital, Pretoria, 0001 South Africa.

<sup>17</sup>Department of Genetics, Center for Molecular Medicine, University Medical Center Utrecht, Utrecht University, Utrecht, 3508 AB The Netherlands.

<sup>18</sup>Department of Clinical Genetics, Leiden University Medical Center, Leiden, 2300 RC The Netherlands.

<sup>19</sup>Department of Medical and Molecular Genetics, Indiana University School of Medicine, Indianapolis, IN 46202, USA.

<sup>20</sup>Department of Pediatrics, Reinier de Graaf Ziekenhuis, Delft, 2600 GA The Netherlands.

<sup>21</sup>Department of Neurology, Reinier de Graaf Ziekenhuis, Delft, 2600 GA The Netherlands.

<sup>22</sup>Department of Clinical Genetics, United Laboratories, Tartu University Hospital and Institute of Clinical Medicine, University of Tartu, Tartu, 50406 Estonia.

<sup>23</sup>Department of Genetics, Yale University School of Medicine, New Haven, CT 06510, USA.

<sup>24</sup>Broad Institute of MIT and Harvard, Cambridge, MA 02142, USA.

<sup>25</sup>Department of Medical Sciences, University of Turin, Turin, 10126 Italy.

<sup>26</sup>Italian Institute for Genomic Medicine, Turin, 10126 Italy.

<sup>27</sup>Department of Clinical and Molecular Medicine, Sapienza University, Rome, 00189 Italy.

<sup>28</sup>Division of Medical Genetics, Casa Sollievo della Sofferenza Hospital, IRCCS, San Giovanni Rotondo, 71013 Italy.

<sup>29</sup>Istituto Neuromed, IRCCS, Pozzilli, 86077 Italy.

<sup>30</sup>These authors contributed equally to this work.

<sup>31</sup>Current affiliation: Department of Genetics and Genomic Sciences, The Icahn School of Medicine at Mount Sinai, New York, NY 10029, USA.

<sup>32</sup>Current affiliation: National Institute of Allergy and Infectious Disease, National Institutes of Health, Bethesda, MD 20892, USA.

<sup>33</sup>These authors jointly coordinated this work.

\*Correspondence:

R Frank Kooy, PhD

Department of Medical Genetics,

University of Antwerp,

Prins Boudewijnlaan 43/6 2650 Edegem, Belgium.

Phone: +32 3 275 9760

Email: [frank.kooy@uantwerpen.be](mailto:frank.kooy@uantwerpen.be)

\*\*Correspondence:

Marco Tartaglia, PhD

Genetics and Rare Diseases Research Division

Ospedale Pediatrico Bambino Gesù

Viale di San Paolo 15, 00146 Rome, Italy.

Phone: +39 06 6859 3742

Email: [marco.tartaglia@opbg.net](mailto:marco.tartaglia@opbg.net)

## Email addresses

Elisabetta Flex	<a href="mailto:elisabetta.flex@iss.it"><u>elisabetta.flex@iss.it</u></a>
Simone Martinelli	<a href="mailto:simone.martinelli@iss.it"><u>simone.martinelli@iss.it</u></a>
Van Dijck, Anke	<a href="mailto:anke.vandijck@uantwerpen.be"><u>anke.vandijck@uantwerpen.be</u></a>
Andrea Ciolfi	<a href="mailto:andrea.ciolfi@opbg.net"><u>andrea.ciolfi@opbg.net</u></a>
Serena Cecchetti	<a href="mailto:serena.cecchetti@iss.it"><u>serena.cecchetti@iss.it</u></a>
Elisa Coluzzi	<a href="mailto:elisa.coluzzi@uniroma3.it"><u>elisa.coluzzi@uniroma3.it</u></a>
Luca Pannone	<a href="mailto:luca.pannone@iss.it"><u>luca.pannone@iss.it</u></a>
Cristina Andreoli	<a href="mailto:cristina.andreoli@iss.it"><u>cristina.andreoli@iss.it</u></a>
Francesca Clementina Radio	<a href="mailto:fclementina.radio@opbg.net"><u>fclementina.radio@opbg.net</u></a>
Simone Pizzi	<a href="mailto:simone.pizzi@opbg.net"><u>simone.pizzi@opbg.net</u></a>
Giovanna Carpentieri	<a href="mailto:giovanna.carpentieri@iss.it"><u>giovanna.carpentieri@iss.it</u></a>
Alessandro Bruselles	<a href="mailto:Alessandro.bruselles@iss.it"><u>Alessandro.bruselles@iss.it</u></a>
Giuseppina Catanzaro	<a href="mailto:giuseppina.catanzaro@uniroma1.it"><u>giuseppina.catanzaro@uniroma1.it</u></a>
Lucia Pedace	<a href="mailto:lucia.pedace@opbg.net"><u>lucia.pedace@opbg.net</u></a>
Evelina Miele	<a href="mailto:evelina.miele@opbg.net"><u>evelina.miele@opbg.net</u></a>
Elena Carcarino	<a href="mailto:elena.carcarino@opbg.net"><u>elena.carcarino@opbg.net</u></a>
Xiaoyan Ge	<a href="mailto:xge@bcm.edu"><u>xge@bcm.edu</u></a>
Chieko Chijiwa	<a href="mailto:cchijiwa@cw.bc.ca"><u>cchijiwa@cw.bc.ca</u></a>
ME Suzanne Lewis	<a href="mailto:suzanne.lewis@ubc.ca"><u>suzanne.lewis@ubc.ca</u></a>
Marije Meuwissen	<a href="mailto:marije.meuwissen@uza.be"><u>marije.meuwissen@uza.be</u></a>
Sandra Kenis	<a href="mailto:Sandra.Kenis@uza.be"><u>Sandra.Kenis@uza.be</u></a>
Nathalie Van der Aa	<a href="mailto:Nathalie.VanderAa@uantwerpen.be"><u>Nathalie.VanderAa@uantwerpen.be</u></a>
Austin Larson	<a href="mailto:Austin.Larson@childrenscolorado.org"><u>Austin.Larson@childrenscolorado.org</u></a>
Kathleen Brown	<a href="mailto:Kathleen.Brown@childrenscolorado.org"><u>Kathleen.Brown@childrenscolorado.org</u></a>
Melissa P Wasserstein	<a href="mailto:mwassers@montefiore.org"><u>mwassers@montefiore.org</u></a>
Brian G Skotko	<a href="mailto:bskotko@mgh.harvard.edu"><u>bskotko@mgh.harvard.edu</u></a>
Maria Karayiorgou	<a href="mailto:mk2758@cumc.columbia.edu"><u>mk2758@cumc.columbia.edu</u></a>
J Louw Roos	<a href="mailto:louw.roos@up.ac.za"><u>louw.roos@up.ac.za</u></a>
Koen L Van Gassen	<a href="mailto:K.L.I.vanGassen-2@umcutrecht.nl"><u>K.L.I.vanGassen-2@umcutrecht.nl</u></a>
Marije Koopmans	<a href="mailto:M.Koopmans-10@umcutrecht.nl"><u>M.Koopmans-10@umcutrecht.nl</u></a>
Emilia K Bijlsma	<a href="mailto:E.K.Bijlsma@lumc.nl"><u>E.K.Bijlsma@lumc.nl</u></a>
Gijs WE Santen	<a href="mailto:G.W.E.Santen@lumc.nl"><u>G.W.E.Santen@lumc.nl</u></a>
Daniela QCM Barge-Schaapveld	<a href="mailto:D.Q.C.M.Barge-Schaapveld@lumc.nl"><u>D.Q.C.M.Barge-Schaapveld@lumc.nl</u></a>
Claudia AL Ruivenkamp	<a href="mailto:C.Ruivenkamp@lumc.nl"><u>C.Ruivenkamp@lumc.nl</u></a>
Mariette J.V. Hoffer	<a href="mailto:M.J.V.Hoffer@lumc.nl"><u>M.J.V.Hoffer@lumc.nl</u></a>
Seema R Lalani	<a href="mailto:seemal@bcm.edu"><u>seemal@bcm.edu</u></a>
Haley Streff	<a href="mailto:streff@bcm.edu"><u>streff@bcm.edu</u></a>
William J Craigen	<a href="mailto:wcraigen@bcm.edu"><u>wcraigen@bcm.edu</u></a>
Brett H Graham	<a href="mailto:bregraha@iu.edu"><u>bregraha@iu.edu</u></a>
Annette PM van den Elzen	<a href="mailto:A.vandenElzen@rdgg.nl"><u>A.vandenElzen@rdgg.nl</u></a>
Daan J Kamphuis	<a href="mailto:Daan.Kamphuis@rdgg.nl"><u>Daan.Kamphuis@rdgg.nl</u></a>
Katrin Õunap	<a href="mailto:Katrin.ounap@kliinikum.ee"><u>Katrin.ounap@kliinikum.ee</u></a>
Karit Reinson	<a href="mailto:karit.reinson@kliinikum.ee"><u>karit.reinson@kliinikum.ee</u></a>
Sander Pajusalu	<a href="mailto:Sander.Pajusalu@kliinikum.ee"><u>Sander.Pajusalu@kliinikum.ee</u></a>
Monica H. Wojcik	<a href="mailto:mwojcik@broadinstitute.org"><u>mwojcik@broadinstitute.org</u></a>
Clara Viberti	<a href="mailto:clara.viberti@iigm.it"><u>clara.viberti@iigm.it</u></a>
Cornelia Di Gaetano	<a href="mailto:cornelia.digaetano@unito.it"><u>cornelia.digaetano@unito.it</u></a>

Enrico Bertini	<a href="mailto:enricosilvio.bertini@opbg.net"><u>enricosilvio.bertini@opbg.net</u></a>
Simona Petrucci	<a href="mailto:s.petrucci@css-mendel.it"><u>s.petrucci@css-mendel.it</u></a>
Alessandro De Luca	<a href="mailto:a.deluca@css-mendel.it"><u>a.deluca@css-mendel.it</u></a>
Rossella Rota	<a href="mailto:rossella.rota@opbg.net"><u>rossella.rota@opbg.net</u></a>
Elisabetta Ferretti	<a href="mailto:elisabetta.ferretti@uniroma1.it"><u>elisabetta.ferretti@uniroma1.it</u></a>
Giuseppe Matullo	<a href="mailto:giuseppe.matullo@unito.it"><u>giuseppe.matullo@unito.it</u></a>
Bruno Dallapiccola	<a href="mailto:bruno.dallapiccola@opbg.net"><u>bruno.dallapiccola@opbg.net</u></a>
Antonella Sgura	<a href="mailto:antonella.sgura@uniroma3.it"><u>antonella.sgura@uniroma3.it</u></a>
Magdalena Walkiewicz	<a href="mailto:magdalena.walkiewicz@nih.gov"><u>magdalena.walkiewicz@nih.gov</u></a>
Frank R Kooy	<a href="mailto:frank.kooy@uantwerpen.be"><u>frank.kooy@uantwerpen.be</u></a>
Marco Tartaglia	<a href="mailto:marco.tartaglia@opbg.net"><u>marco.tartaglia@opbg.net</u></a>

## **Abstract**

Histones mediate dynamic packaging of nuclear DNA in chromatin, a process that is precisely controlled to guarantee efficient compaction of the genome and proper chromosomal segregation during cell division, and accomplish DNA replication, transcription and repair. Due to these important structural and regulatory roles, it is not surprising that histone functional dysregulation or aberrant expression can have severe consequences for multiple cellular processes that ultimately might contribute to cell transformation or affect development. Recently, germline frameshift mutations involving the C-terminal tail of HIST1H1E, a widely expressed member of the linker histone family facilitating higher order chromatin folding, have been causally linked to an as yet poorly-defined syndrome with intellectual disability. We report that these mutations result in stable proteins that reside in the nucleus, bind to chromatin, disrupt proper compaction of DNA, and are associated with a specific methylation pattern. Cells expressing these mutant proteins have a dramatically reduced proliferation rate and competence, hardly enter into the S phase, and undergo accelerated senescence. Remarkably, clinical assessment of a relatively large cohort of subjects sharing these mutations revealed a premature aging phenotype as a previously unrecognized feature of the disorder. Our findings identify a direct link between aberrant chromatin remodeling, cellular senescence and accelerated aging.

## Introduction

In eukaryotic cells, nuclear DNA is organized in a complex and dynamical structure called chromatin, which allows efficient packaging of the genome and proper chromosomal segregation during mitosis, and controls its accessibility for essential processes, such as replication, transcription and repair.<sup>1</sup> The basic unit of chromatin is the nucleosome, in which a stretch of about 147 bp of DNA wraps around an octamer of the core histones (*i.e.*, H2A, H2B, H3 and H4), constituting the nucleosomal core particle (NCP).<sup>2</sup> A number of H1 linker histone isoforms bind to short DNA segments at the entry and exit sites on the surface of the NCP, stabilizing the nucleosomal structure and contributing to higher order chromatin folding.<sup>3,4</sup> While H1 histones have traditionally been associated with chromatin compaction and a regulatory function favoring transcriptional repression,<sup>5</sup> a more complex and plastic role of these proteins in the control of accessibility to DNA has gradually been appreciated.<sup>6-8</sup> In mammals, H1 histones are encoded by 11 genes. Among these, seven are expressed in somatic cells, while the remaining four are transcriptionally active in the germline.<sup>3,4</sup> Of note, even among the seven somatic subtypes, the levels of these proteins appears to be regulated during the cell cycle, development and in different tissues and cell types, suggesting specific function of individual isoforms.<sup>9</sup> On the other hand, redundancy in their function has been reported.<sup>10,11</sup> In higher eukaryotes, H1 histone isoforms share a tripartite structure consisting of a central highly conserved globular domain and two less conserved, unstructured *N*-terminal and *C*-terminal tails. The globular domain has high sequence homology among H1 subtypes and mediates binding to the nucleosome. The two tails are moderately conserved among orthologs but differ among isoforms, suggesting functional specificity. Notably, both tails encompasses a number of residues subjected to reversible modifications with regulatory function. Among these, the extent of phosphorylation in serine/threonine residues at the *C*-terminal tail has been proposed to regulate chromatin dynamics in interphase as well as chromosome condensation during mitosis.<sup>4,12</sup>

Aberrant histone function, whether due to mutations in genes coding proteins participating in histone-modifying complexes or mutations directly affecting histone-coding genes, has been established to contribute to oncogenesis and cause multisystem syndromes affecting growth and cognitive function.<sup>13-18</sup> Recently, while this work was underway, germline frameshift mutations affecting *HIST1H1E* (MIM: 142220), coding a member of the somatic, replication-dependent linker histone subfamily, have been causally linked to an as yet poorly-defined syndrome with intellectual disability (ID) (MIM: 617537).<sup>19</sup> Mutations mapped at the C-terminal tail of HIST1H1E and were predicted to have an equivalent functional impact by generating the same change in the reading frame. The five affected individuals belonged to a cohort of subjects with overgrowth, and were reported to have a similar facial appearance, but variable height, head circumference and degree of ID.<sup>19</sup> Notably, the growth pattern of these individuals appeared complex and characterized by an above-average height during infancy progressively decreasing over time, resulting in an average/short stature in adulthood. This peculiar pattern of growth has been highlighted by a subsequent report, which also confirmed the association of this class of *HIST1H1E* mutations with ID and specific facial features.<sup>20</sup>

Here, we report that this homogeneous class of disease-causing frameshift mutations affecting the C-terminal tail of HIST1H1E results in stable proteins that reside in the nucleus and bind to chromatin but disrupt proper compaction of DNA, and are associated with a specific methylation profile. We also provide data indicating that cells expressing these mutant proteins have a dramatically reduced proliferation rate and competence, hardly enter into the S phase, and undergo accelerated senescence. Remarkably, clinical assessment of 13 newly identified individuals heterozygous for this class of mutations and those previously reported allowed to identify premature aging as a previously unrecognized feature of the disorder. Collectively, these data highlight a strict link between aberrant chromatin remodeling, cellular senescence and accelerated aging.



## **Subjects and Methods**

### **Subjects**

This study was approved by the Committee for Medical Ethics, University of Antwerp, Antwerp, and Ethical Committee, Ospedale Pediatrico Bambino Gesù, Rome. Clinical data and DNA specimens from the subjects included in this study were collected following procedures in accordance with the ethical standards of the declaration of Helsinki protocols and approved by the Review Boards of all involved institutions, with signed informed consents from the participating subjects/families. Explicit permission was obtained to publish the photographs of the subjects as shown in Figure 1.

### **Exome sequencing**

WES was performed using DNA samples obtained from leukocytes. In most cases, a trio-based strategy was used. Exome capture was carried out using the Nimblegen SeqCap EZ Exome v3 (Roche) (subjects 1 and 5), SeqCap EZ VCRome v2.1 (Roche) (subjects 6 and 7), SureSelect Human All Exon v4 (Agilent) (subjects 2, 3, 8, 9 and 13), SureSelect Human All Exon v5 (Agilent) (subjects 4 and 12), SureSelect XT Human All Exon v6 (Agilent) (subjects 10 and 11) target enrichment kits, and sequencing was performed on HiSeq 2000/2500/4000 and NexSeq550 platforms (Illumina), using paired-end reads. WES data processing, sequence alignment to GRCh37, and variant filtering and prioritization by allele frequency, predicted functional impact, and inheritance models were performed as previously described.<sup>21-27</sup> The *de novo* origin of the *HIST1H1E* frameshifts was confirmed by Sanger sequencing in all cases.

### **RNA stability**

Total RNA was isolated from circulating leukocytes of subjects 1 and 2 (S1 and S2, hereafter) by RNeasyMiniKit (Qiagen). Reverse transcription was performed using the SuperScriptIII first strand kit (Invitrogen), following the manufacturer's instructions. Primer sequences used to perform the RT-PCR are available upon request.

### **Constructs**

The c.441dupC (p.Lys148GlnfsTer48), c.464dupC (p.Lys157GlnfsTer39) and c.441\_442insCC (p.Lys148ProfsTer82) were introduced by site-directed mutagenesis in a *HIST1H1E* cDNA (RefSeq: NM\_005321.2, NP\_005312.1) tagged with Xpress at the *N*-terminus cloned in pcDNA6/His version C (Invitrogen).

### **Cell Cultures and transfections**

Skin fibroblasts isolated from skin biopsy (subjects S1 and S2 and healthy donors), and COS-1 and HeLa lines were cultured in Dulbecco's modified Eagle's medium supplemented with 10 % heat-inactivated fetal bovine serum (Gibco) and 1 % penicillin-streptomycin, at 37 °C with 5% CO<sub>2</sub>.

### **SCGE assay**

Samples were processed according to the alkaline SCGE assay protocol, as previously described.<sup>28</sup> Briefly, cells were suspended in 0.7 % low melting agarose. Slides were prepared in duplicates with control cells and fibroblasts derived from affected individuals placed on opposite sides of the same slide, immersed in cold lysis solution and kept at 4 °C overnight. After lysis, slides were transferred in alkaline buffer for 20 min. Electrophoresis was carried out for 20 min at 20 V and 300 mA (0.8 V/cm) at 4 °C. Basal level of nucleoids relaxation was explored applying longer electrophoresis run-times (40 and 60 min). Slides were neutralized in 0.4 M Tris (pH 7.5) for 5 min, treated with absolute ethanol and stored at room temperature. Slides were then stained with GelRed (Biotium Inc) and scored at a fluorescence microscope (Leica). To evaluate induced DNA damage and DNA repair capability, fibroblasts were irradiated with 1 or 2 Gy  $\gamma$ -rays from a <sup>137</sup>Cs source at a dose rate of 0.8 Gy/min. During treatment, cells were maintained at 0 °C to prevent DNA repair. The kinetics of DNA repair were assessed by SCGE assay, as described above. The residual DNA damage was measured after 15 and 30 min of incubation at 37 °C. For each experimental point, at least 75 cells were analyzed.

### **Histone modifications and nucleolus morphology assessment**

For immunofluorescence, fibroblasts from S1 and control subjects were seeded at a density of  $20 \times 10^3$  in 24-well cluster plates onto 12-mm cover glasses. After 24 h of culture in complete

medium, cells were fixed with 3 % paraformaldehyde. Following permeabilization with 0.5 % Triton X-100 (10 min at room temperature), fibroblasts were stained with anti-dimethyl-Histone H3 (lys4) rabbit polyclonal antibody, anti-trimethyl-histone H3 (lys9) rabbit polyclonal antibody, anti-trimethyl-histone H3 (lys27) rabbit polyclonal antibody (Millipore), anti-heterochromatin protein-1 $\beta$  mouse monoclonal antibody (Chemicon) followed by the appropriate secondary antibody (Invitrogen) and DAPI. To study nucleolus morphology, fibroblasts were stained with C23 (MS-3) mouse monoclonal antibody (Santa Cruz) followed by the appropriate secondary antibodies (Invitrogen) and DAPI. Observations were performed on a Leica TCS SP2 AOBS apparatus. Cells stained only with the fluorochrome-conjugated secondary antibodies were used to set up acquisition parameters. Signals from different fluorescent probes were taken in sequential scanning mode, several fields (>200) were analyzed for each labeling condition, and representative results are shown.

### **Proliferation and cell cycle assays**

Cells were seeded at 200.000 cells/well in a 6-well plate and incubated at 37 °C. Cell numbers (mean of three replicates  $\pm$  SD) were counted by trypan blue exclusion after four and seven days. The percentage of cells in different cell cycle phases was determined by dual flow cytometry analysis of BrdU-positive cells and stained with the fluorescent DNA probe propidium iodide. Briefly, cells were incubated for 1 h with BrdU (Sigma Aldrich) at a final concentration of 30  $\mu$ M. Then BrdU was removed, cells were rinsed with PBS prior to harvesting and permeabilized using ice-cold 100 % EtOH. Cells were incubated with HCl 3N to denature DNA and 0.1 M sodium tetraborate to stop this reaction. Fibroblasts were incubated with the anti-BrdU antibody (Invitrogen) followed by goat anti-mouse Alexa Fluor 488 secondary antibody. Finally, cells were resuspended in a buffer containing 10  $\mu$ g/ml RNase A and 20  $\mu$ g/ml propidium iodide and immediately analyzed by FACSCalibur (BD Biosciences).

### **SA- $\beta$ -gal activity and P53 evaluation**

SA- $\beta$ -gal activity was assessed as reported.<sup>29</sup> Briefly, cells were fixed with 3.6 % formaldehyde in PBS for 4 min at room temperature. Fixed cells were washed and incubated overnight with freshly-prepared staining solution at 37 °C in the absence of CO<sub>2</sub>. After washing, the coverslips were mounted by using the antifade Dako fluorescence mounting medium (Agilent Technologies). P53 endogenous levels were evaluated on fibroblast lysates collected at different passages using an anti-p53 mouse monoclonal antibody (Invitrogen). Membranes were probed with an anti-GAPDH mouse monoclonal antibody (Santa Cruz) to normalize protein content.

### **Analysis of nuclear morphology**

After 24 h of culture in complete medium, fibroblasts were treated with 2 mM thymidine (Sigma) for 24 h, washed with 1X PBS, recovered with complete medium for 3 h and then treated with 100 ng/ml nocodazole (Sigma) for 12h. Afterwards, fresh drug-free medium was added and recovery was allowed for 120 min, by fixing the cells every 15 min using PHEMO buffer for 10 min at room temperature, as previously described.<sup>30</sup> Finally, cells were stained with lamin A/C mouse monoclonal antibody (Santa Cruz) followed by the appropriate secondary antibody (Invitrogen) and DAPI. Observations were performed on a Leica TCS SP2 AOBS apparatus as described above.

### **Evaluation of rRNA content**

Total RNA was extracted from the same amount of control fibroblasts and cells derived from affected subjects (400,000 fibroblasts) at different cellular passages. Three  $\mu$ l of total RNA was loaded for size separation on 1 % agarose gel and stained with ethidium bromide.

### **Evaluation of protein stability**

COS-1 cells were seeded in 6-well plates the day before transfection. Monolayer were transfected at 70 % confluency with Fugene 6 transfection reagent (Promega) with wild-type or mutant Xpress-tagged *HIST1H1E* expression constructs. Forty-eight h after transfection, cells were treated with cycloheximide (20  $\mu$ g/ml) for 8 and 16 h, or left untreated before lysis. Xpress-tagged HIST1H1E levels were assessed by immunoblotting. Membranes were probed with an anti-GAPDH antibody (Santa Cruz) to normalize protein content.

### **CSK assay**

Twenty thousand fibroblasts and  $30 \times 10^3$  HeLa cells were seeded on glass coverslip and maintained in culture complete medium for 24 h. HeLa cells were transfected with 100 ng of vectors expressing Xpress-tagged HIST1H1E. Forty-eight h after transfection, HeLa cells were either fixed with 3 % paraformaldehyde, or treated with CSK buffer before being fixed.<sup>31</sup> After permeabilization with 0.5 % TritonX-100 (10 min at room temperature), HeLa cells were stained with monoclonal antibody to Xpress (Invitrogen) followed by the appropriate secondary antibody (Invitrogen) and DAPI for DNA. Analyses were performed in three independent experiments on a Leica TCS SP2 AOBS apparatus.

### **Analysis of cell morphology**

Fibroblasts from subject S1 and a control individual were seeded in a 100 mm dish cell culture. Optical microscope images at different passages were taken with Fluid Cell Imaging Station (Life Technologies).

### **$\gamma$ H2AX immunofluorescence staining**

Cells were seeded on a glass in a petri dish for 24 h. The slides were fixed with 4 % paraformaldehyde (Sigma Aldrich), permeabilized in 0.2 % Triton X-100 and blocked in PBS/BSA 1 % for 30 min at room temperature. Slides were incubated with a mouse mono-clonal anti-phospho-histone H2AX antibody (Millipore) overnight at 4 °C, washed in PBS/BSA 1 % and then exposed to the secondary Alexa 488-labelled donkey anti-mouse antibody (Invitrogen, Life Technologies) for 1 h at 37 °C. After washes in PBS/BSA, 1 % DNA were counterstained by DAPI (Sigma Aldrich) in Vectashield (Vector Laboratories). Cells were analyzed with fluorescence microscopy using an Axio Imager Z2 microscope (Zeiss). The frequency of foci per cell were scored in 150 nuclei in two independent experiments.

### **Telomere dysfunction-induced foci (TIF) immunoFISH staining**

Cells were seeded on glass slides that were processed as reported for the  $\gamma$ H2AX immunofluorescence staining up to the secondary antibody (Alexa 488-labelled donkey anti-mouse,

Invitrogen). Immediately after, slides were washed in PBS/Triton X-100 0.05 %, fixed in 4 % formaldehyde for 2 min and dehydrated through graded alcohols (70 %, 80 % and 100 %). Slides and probes (Cy3 linked telomeric PNA probe, DAKO) were co-denatured at 80 °C for 3 min and hybridized for 2 h, at room temperature in a humidified chamber. After hybridization, slides were washed twice for 15 min in 50% formamide, 10 mM Tris, pH 7.2, and 0.1 % BSA followed by three 5 min washes in 0.1 M Tris, pH 7.5, 0.15 M NaCl and 0.08 % Tween 20. Slides were then dehydrated with an ethanol series and air dried. Finally, slides were counterstained with DAPI (Sigma Aldrich) in Vectashield (Vector Laboratories). Co-localisation between  $\gamma$ H2AX foci and telomere, were analysed using an Axio Imager Z2 microscope (Zeiss). The frequency of co-localisation dots per cell were scored in 150 nuclei in two independent experiments.

#### **Quantitative-fluorescence “in situ” hybridization analysis (Q-FISH)**

Chromosome spreads were obtained as reported above. Q-FISH staining was performed as previously described,<sup>32</sup> with minor modifications. Briefly, slides and probes (Cy3 linked telomeric, PANAGENE, and chromosome 2 centromeric PNA probes, DAKO) were co-denatured at 80 °C for 3 min, and hybridized for 2 h at room temperature in a humidified chamber. Slides were counterstained with DAPI (Sigma Aldrich) in Vectashield (Vector Laboratories). Images were captured at a 63X magnification with an Axio Imager Z2 (Zeiss). The ISIS software (MetaSystems) was used to assess the telomere size (defined as ratio between total telomeres fluorescence [T] and fluorescence of the centromere of the two chromosomes 2 [C]). Data were expressed as T/C %.<sup>33</sup> Experiments were repeated two times, and at least 10-15 metaphases were scored each time.

#### **Detection of aneuploidy**

Chromosome spreads were obtained as described before. Metaphases were captured at 63X magnification with an Axio Imager Z2 microscope (Zeiss). We considered euploidy the metaphases with 46 chromosomes and aneuploidy all the metaphases that had a different number of chromosome. The frequency of aneuploidy was scored in 40 metaphases. Two independent experiments were performed.

### **Chromosome condensation assay**

After 30 min incubation with 30  $\mu$ M Calyculin-A (Wako), a 28 min incubation at 37 °C with hypotonic solution (75 mM KCl) and fixation in freshly prepared Carnoy solution (3:1 v/v methanol/acetic acid), chromosome spreads were obtained. Slides were stained with DAPI (Sigma Aldrich) in Vectashield (Vector Laboratories) and an Axio Imager Z2 microscope (Zeiss) was used. To analyze the frequency of chromosomal condensation we counted the number of metaphases in 150 nuclei per sample in two independent experiments.

### **Methylome profiling**

DNA methylation levels of one adult and 5 pediatric affected subjects were analyzed using genomic DNA extracted from leucocytes by the Infinium Human Methylation EPIC BeadChip assay (Illumina) to allow comprehensive genome-wide coverage. Methylation levels were measured as Beta-values, or percentage of methylation at each CpG site, ranging from 0 (*i.e.*, no methylation) to 1 (full methylation). Raw data were processed with Bioconductor package ChAMP,<sup>34</sup> using default parameters to filter low-quality signals and normalize data. Methylation profiles were compared with those obtained from a series of 35 healthy adult male controls of European descent, including 31 subjects selected from a European cohort study (average age  $\pm$  SD: 56.1  $\pm$  7.4 years),<sup>35</sup> using unsupervised multidimensional scaling (MDS) analysis, taking into account the 1,000 most variable probes amongst samples. Statistical analyses were conducted using R software (V. 3.5.0). Gene and Pathway Enrichment analyses of the differentially methylated probes were performed using WEB-based Gene Set Analysis online tool,<sup>36</sup> on the associated genes. Functional annotation was carried out by means of GO terms, including biological processes, molecular functions and cellular components classes. Pathway analysis was performed using KEGG. Statistical significance was assumed at 0.05, following multiple testing adjustment (FDR).

## **Results**

### **Spectrum of *HIST1H1E* mutations and associated clinical features**

Using whole-exome sequencing (WES), we identified a novel *de novo* *HIST1H1E* frameshift variant, c.441dupC (p.Lys148GlnfsTer48), in an adult individual with hypotrichosis, cutis laxa, and ID (Figure 1A). Mutation analysis performed on primary skin fibroblasts and hair bulb epithelial cells of the affected subject supported the germline origin of the frameshift. The variant had not been reported in ExAC/gnomAD, and affected a relatively large portion of the encoded protein highly conserved among orthologs. In the subject, WES data analysis excluded the presence of other functionally relevant variants compatible with known Mendelian conditions based on the expected inheritance model and clinical presentation. Through networking and GeneMatcher search,<sup>37</sup> we identified 12 additional subjects with similar *de novo* frameshift *HIST1H1E* mutations (Figure 1B, Table 1). All changes were short out-of-frame indels resulting in almost identical shorter proteins containing a shared divergent C-terminal tail (Table S1), which was consistent with previous reports.<sup>19,20,38,39</sup> None of the frameshifts had been reported in gnomAD, all were predicted to dramatically impact protein function, and two of them had already been reported in ClinVar as disease-causing mutations (Table 1).

We analyzed the clinical records of the 13 identified subjects (S1 to S13) and collected the information available for the seven previously published individuals (S14 to S20). All subjects had variable developmental delay (DD)/ID and a distinctive facies characterized by bitemporal narrowing (100%), prominent forehead (93%) and high anterior hairline (88%) as main features, which were reminiscent of Pallister-Killian syndrome (MIM: 601803) (Figure 1A). In four children, Sotos syndrome (MIM: 117550) had been suggested, while Weaver syndrome (MIM: 277590), Simpson-Golabi-Behmel syndrome (MIM: 312870) and Pallister-Killian syndrome had been suspected in single cases (Table S2). Half of the individuals had scaphocephaly and sparse frontotemporal hair. The craniofacial appearance was characterized by hypertelorism (91% of individuals), downslanted palpebral fissures (67%), broad nasal tip (83%), and low-set and posteriorly rotated ears (57%). Forty-three percent of subjects showed small, widely spaced teeth. Skin hyperpigmentation was present in one third of individuals. Neonatal problems included



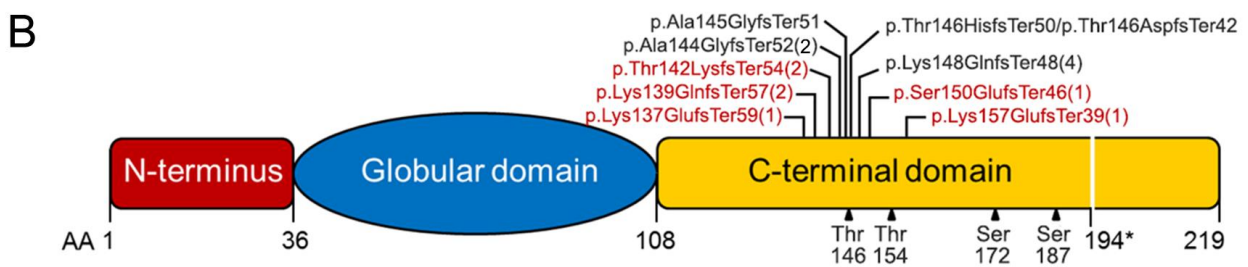


**Figure 1. Facial appearance of subjects with HIST1H1E frameshift mutations and protein structure (A)** In affected subjects, facial appearance is characterized by a high anterior hairline, prominent forehead, bitemporal narrowing, sparse temporal hair, hypertelorism, hooded eyelids, short palpebral fissures, high and broad nasal bridge with full nasal tip, small, widely spaced teeth, and low-set ears. A facial appearance compatible with a more advanced age (e.g., hypotrichosis and ptosis) is evident in S1 and S3 (S1, 49 yrs; S3, 30 yrs; S4, 14 months; S5, 12yrs; S6, 3yrs; S7, 12yrs; S9, 2yrs; S11, 6yrs; S12, 4yrs). **(B)** Schematic diagram representing the HIST1H1E structure, which is composed by a globular domain flanked by N- and C-terminal tails. The position of the disease-causing frameshift mutations is shown above the cartoon (novel mutations are highlighted in red). The number of independent cases identified in the present study is in brackets. The domain boundaries and cyclin-dependent kinase phosphorylation sites (black triangles) are reported below the cartoon. All mutations are expected to result in a shorter protein with an identical divergent C-terminal tail (the new stop codon is shown below the cartoon, 194\*).

**Table 1. Frameshift *HIST1H1E* mutations identified in this study.**

Nucleotide Change	gnomAD	ClinVar	Amino acid change	Domain	CADD <sup>1</sup>	Number of cases	Origin
c.408dupG	-	-	p.Lys137GlufsTer59	C-terminal tail	34	1	<i>de novo</i>
c.414dupC	-	-	p.Lys139GlnfsTer57	C-terminal tail	35	2	<i>de novo</i> (1)
c.425_431delinsAGGGGGT	-	-	p.Thr142LysfsTer54	C-terminal tail	31	1	<i>de novo</i>
c.425delinsAG	-	-	p.Thr142LysfsTer54	C-terminal tail	29	1	undetermined
c.430dupG	-	reported	p.Ala144GlyfsTer52	C-terminal tail	26.8	2	undetermined
c.441dupC	-	reported	p.Lys148GlnfsTer48	C-terminal tail	34	4	<i>de novo</i>
c.447dupG	-	-	p.Ser150GlufsTer46	C-terminal tail	34	1	<i>de novo</i>
c.464dupC	-	-	p.Lys157GlufsTer39	C-terminal tail	35	1	<i>de novo</i>

Nucleotide numbering reflects cDNA numbering with 1 corresponding to the A of the ATG translation initiation codon in the *HIST1H1E* reference sequence (RefSeq: NM\_005321.2, NP\_005312.1).

<sup>1</sup> CADD v1.4.

hypotonia, feeding difficulties, failure to thrive, jaundice, congenital hypothyroidism, and micrognathia. Three showed single palmar creases possibly related with prenatal hypotonia. Finger abnormalities included short fourth metacarpals, camptodactyly, fifth finger clinodactyly, brachydactyly, broad and low-set thumbs. Toe abnormalities included long halluces, broad toes and fifth toes overlapping fourth toes. Two individuals had pectus excavatum. Growth parameters at birth were unremarkable. At last evaluation, only one subject (S10) had macrosomy ( $> 3.65$  SD), while 12 individuals (63%) had a large head circumference ( $> +2.0$  SD), including two children with relative macrocephaly at the age of 4 years. Developmental delay was present in all individuals. They were mildly to moderately intellectually disabled. Fourteen cases have speech delay, and gross motor delay was a common feature. In young individuals, hypotonia and a stiff, clumsy and uncoordinated gait were relatively common findings. The 49-year-old individual (S1) had gait ataxia. Behavioral features include ADHD (two individuals), autistic features (five individuals), and psychotic episodes (one individual). One child had focal seizures in early childhood, another child was treated for recurrent status epilepticus. Brain MRI reveals aspecific abnormalities like mild inferior vermian hypoplasia, delayed myelination, partial agenesis of the corpus callosum, and mild to moderately enlarged third and lateral ventricles. Five individuals presented with mild hearing loss. Visual problems included hypermetropia, myopia, astigmatism, and strabismus. Sixty percent of the individuals had feeding or eating difficulties, ranging from satiety problems at younger age to problems swallowing fluids or learning to eat solid food. One child was fed by G-tube at the age of 2.5 years. She had gastro-esophageal reflux disease and rumination disorder. Other remarkable features in this cohort include pancytopenia accompanying systemic lupus erythematosus in the oldest individual. A summary of the major features are reported in Table 2, while a more detailed description for each subject is available in Table S2.

Notably, the oldest individuals of the present cohort (S1 and S3) and two previously reported subjects (S15 and S17) had a facial appearance compatible with a much more advanced age. When we evaluated the clinical presentation of the entire cohort of affected individuals,

**Table 2. Summary of the clinical features occurring in subjects carrying *de novo* HIST1H1E frameshift mutations.**

Clinical features	Frequency <sup>1</sup>
<b>DD/ID</b>	<b>18/18<sup>2</sup> (100%)</b>
Motor delay	12/12 (100%)
Walking independently, range (mean), months	15-66 (31)
Speech delay	14/14 (100%)
Hypotonia	11/15 (73%)
Autistic features	5/14 (36%)
<b>Craniofacial features</b>	<b>19/19 (100%)</b>
Macrocephaly	12/19 (63%)
Scaphocephaly	6/11 (54%)
Sparse hair	6/12 (50%)
High anterior hairline	14/16 (87%)
Prominent forehead	13/14 (93%)
Hypertelorism	10/11 (91%)
Downslanted palpebral fissures	8/12 (67%)
Full nasal tip	10/12 (83%)
Low set ears	8/14 (57%)
<b>Aging appearance</b>	<b>20/20 (100%)</b>
Skin hyperpigmentation	5/15 (33%)
Hypotrichosis	6/20 (30%)
Skin hyperpigmentation	5/20 (25%)
Nail abnormalities	6/20 (30%)
Dental problems	6/20 (30%)
Advanced bone age	4/20 (20%)
<b>Other</b>	<b>9/15 (60%)</b>
Feeding or eating difficulties	9/15 (60%)
Hearing loss	5/14 (36%)
Strabismus	8/15 (53%)

<sup>1</sup> The reported cohort includes 13 presently described subjects and 7 previously reported cases.

<sup>2</sup> Subjects showed variable ID: 5 mild, 9 moderate, and 2 severe. In 2 cases the severity of ID was unspecified.

including those previously reported, we noticed an overrepresentation of features that are generally less common for individuals in this age group but more commonly found in elderly subjects, including hypotrichosis, ptosis, cutis laxa, hyperkeratosis, skin hyperpigmentation, dry skin, nail abnormalities, hearing loss, cataracts, diabetes mellitus and osteopenia (Table S3). One girl was diagnosed with childhood hypophosphatasia (osteopenia and advanced bone age that was investigated after presenting with multiple small stress fractures of the lower limbs). Three other children also had advanced bone age. A fifth child has multiple fractures after minor trauma. Several children had dental problems including missing permanent teeth and small, fragile teeth.

### **Functional characterization of *HIST1H1E* mutations**

Based on the unique narrow spectrum of mutations, we hypothesized a specific disruptive impact on *HIST1H1E* function as a consequence of the frameshift. Haploinsufficiency was considered unlikely since endogenous *HIST1H1E* mRNA levels from two unrelated affected subjects (S1, 49 yrs; S2, 4 yrs) were comparable to controls and transient transfection experiments using Xpress-tagged *HIST1H1E* constructs in COS-1 cells documented an increased stability of the mutant proteins compared to the wild-type protein (Figure S1). Furthermore, confocal microscopy analysis performed in transiently transfected HeLa cells showed proper nuclear localization and stable binding to chromatin of the tested mutants (Figure S2). These data and the finding that a mutant generated to express the third open reading frame at an equivalent position of the C-terminus (not occurring in affected subjects) was characterized by compromised chromatin binding indicating loss-of-function (Figure S2), strongly suggested a dominant negative or neomorphic effect as the mechanism of disease.

H1 linker histones are core chromatin components, and bind to short DNA segments at the entry/exit sites on the surface of nucleosomes, stabilizing their structure and regulating chromatin folding.<sup>4</sup> The C-terminal tail of H1 histones contains a number of serine/threonine residues that undergo reversible phosphorylation, modulating the dynamics of chromatin compaction, which are lost in disease-associated *HIST1H1E* mutants. Of note, while partial phosphorylation of the C-

terminal tail allows chromatin relaxation during interphase, full phosphorylation is required for maximal chromatin condensation during mitosis.<sup>4,12</sup> To assess chromatin compaction, single cell gel electrophoresis (SCGE) assay was performed in primary fibroblasts from subjects S1 and S2. Increasing run times performed to allow DNA loops to extend under the electrophoretic field showed a significantly increased nucleoid relaxation in fibroblasts from affected individuals compared to control cells, quantified as “tail moment” values (Figure 2A). Since chromatin compaction is associated with a specific pattern of histone modifications, including methylation of histone H3 at specific lysine residues,<sup>40</sup> the methylation profile of histone H3 was assessed in the two fibroblast lines. Consistent with the SCGE data, a decrease in H3K4me2, H3K9me3, and H3K27me3 staining was documented by immunofluorescence analyses (Figure 2B). In line with these findings, reduced levels of HP1 $\beta$ , a member of the HP1 family mediating heterochromatinization by binding to methylated H3K9, and whose expression is reduced in cells with a defective heterochromatin state,<sup>41</sup> was also observed (Figure 2C). Finally, a caliculin-induced premature chromosome condensation assay documented a significant reduction of condensed chromosomes in fibroblasts from affected subjects (11.3 % of analyzed cells) compared to control cells (19.6 %) ( $P < 0.01$ ,  $\chi^2$  test). Overall, these data indicated a more relaxed state of chromatin in cells expressing the disease-causing HIST1H1E mutants.

### **Methylome profiling**

Since altered chromatin condensation is expected to impact DNA methylation,<sup>42</sup> a genome-wide methylation profiling analysis was used to investigate perturbations at the epigenome level. To this aim, a subset of DNA samples obtained from leukocytes of six affected subjects were compared to those referring to a control group including 35 healthy individuals of European descent by Infinium MethylationEPIC BeadChip profiling. Considering the entire set of assayed target probes, the analysis did not highlight a substantial change in methylation pattern (data not shown). However, multidimensional scaling analysis carried out considering the information associated to the 1,000 most differentially methylated probes among all samples (independently from their group

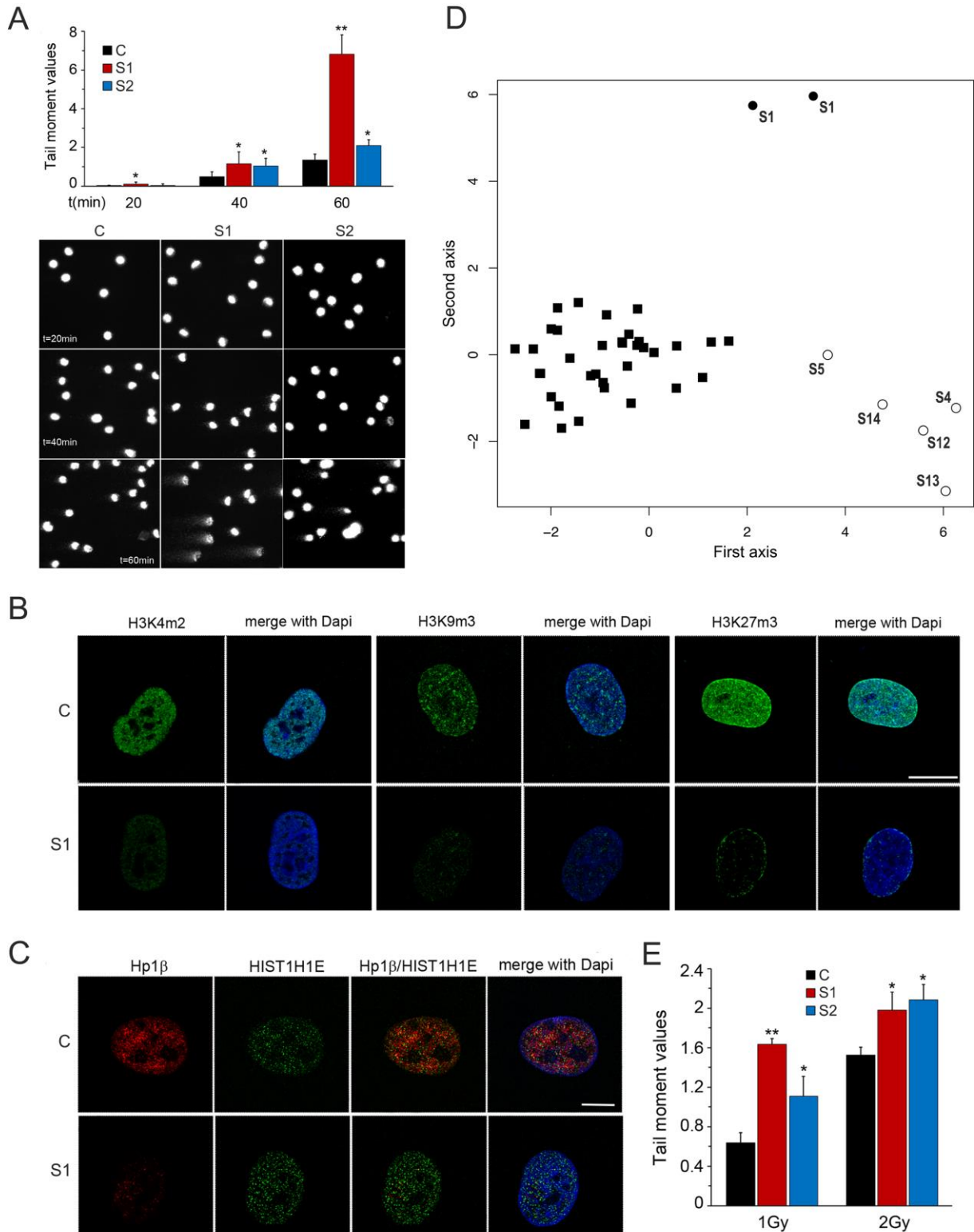


**Figure 2. SCGE assay, immuno-fluorescence studies, and methylation profiling analysis** (A) Increasing electrophoresis run times (20, 40 and 60 min) highlighted significant differences in relaxation of DNA supercoiling between fibroblasts from control and affected subjects. DNA migration was quantified as Tail moment values, which is defined as the product of the tail length and the fraction of total DNA in the tail (upper panel). Nucleoids of cells from subjects S1 and S2 showed a significantly higher Tail moment value ( $*P < 0.05$ ,  $**P < 0.01$ ; two-tailed Student's t-test). For each experimental point, at least 75 cells were analyzed. Values are mean  $\pm$  SEM of three independent experiments. Representative images of nucleoids from fibroblasts from control and affected individuals at each run time are shown (lower panel). (B) Confocal laser scanning microscopy (CLSM) observations document an overall decreased amount of H3K4me2, H3K9me3, and H3K27me3 staining (green) in S1 cells compared to control cells. Nuclei were stained with DAPI. Images are representative of  $>200$  analyzed cells. Bars correspond to 8  $\mu$ m. (C) Fibroblasts from subject S1 show a decreased amount of HP1 $\beta$  compared to control cells (WT). Cells were stained using antibodies against HP1 $\beta$  (red) and HIST1H1E (H1.4) (green); DNA are DAPI-stained (blue). Scale bars represent 7  $\mu$ m. (D) Multidimensional scaling plot of genome-wide methylation analysis using the top 1,000 most variable probes among samples. The plot shows the distinct methylation profiles of pediatric (open circles) and adult (S1, duplicate) (filled circles) affected subjects, compared to healthy controls (filled squares). (E) DNA damage was induced by 1 or 2 Gy  $\gamma$ -ray irradiation. Tail moment values indicate the amount of radiation-induced DNA damage measured by SCGE assay immediately after treatment. S1 and S2 fibroblasts showed a higher sensitivity to  $\gamma$ -ray irradiation ( $*P < 0.02$ ,  $**P < 0.001$ ; two-tailed Student's t-test). For each experimental point, at least 75 cells were analyzed. Values are mean  $\pm$  SEM of three independent experiments.

classification) indicated clear-cut divergent methylation profiles between healthy controls and affected individuals, the latter clustering according to the age of subjects (Figure 2D). Among these informative probes, 170 differentially methylated CpGs were located within the UCSC CpG Islands (from 200bp to 1500bp from TSS) (Table S4). KEGG and GO Cellular Component enrichment analyses revealed a significant enrichment of genes linked to pathways mainly related to neurological, immunological, and cell adhesion/membrane function, which represent cellular processes relevant to the clinical phenotype of affected subjects (Table S5). A separate clustering of affected pediatric individuals from controls was also observed by using a recently defined episinature set modeled to successfully profile 14 developmental disorders (data not shown),<sup>43</sup> further supporting the occurrence of a specific methylation profile in subjects with *HIST1H1E* frameshift mutations. These findings are in line with previous studies performed in cells with defective histone H1 function documenting a minor impact on global DNA methylation. In these cells, changes rather involved specific CpGs within regulatory domains of regulated genes,<sup>44</sup> indicating that chromatin rearrangement in these cells does not impact globally the methylation status of DNA, but affects specific subsets of genes and cellular processes.

### ***HIST1H1E* mutations cause accelerated cellular senescence**

Based on the occurrence of phenotypic features suggestive of premature aging and the fact that a more relaxed compaction of chromatin has been functionally linked to replicative senescence,<sup>45</sup> a feature occurring in progeroid syndromes,<sup>46</sup> we hypothesized that the aberrant function of the *HIST1H1E* mutants might promote accelerated senescence. To test this hypothesis, proliferative competence and morphological and biochemical markers of cellular senescence were evaluated. Trypan blue exclusion assay documented a variable but consistently reduced proliferation rate in cells from affected subjects (Figure 3A). Of note, a complete proliferative arrest was observed in S1 fibroblasts at relatively early passages. Consistent with this finding, flow cytometry analysis documented a block in cell cycle transition from G0/G1 to S phase (Figure 3B). Compared to control fibroblasts, those derived from affected individuals were larger and had a flattened and



**Figure 3. Proliferation assay and cell cycle progression.** (A) Cells were seeded at 200,000 cell/well in a 6-well plate and incubated at 37 °C. Cell numbers (mean of three replicates  $\pm$  SD) were counted by Trypan blue exclusion assay after four and seven days. A significantly decreased proliferation rate was observed in the fibroblast lines from the two unrelated affected individuals (S1 and S2). Cells from subject S1 show a permanent cells growth arrest. (B) Cell cycle phases of S1/S2's (right) and control (left) fibroblasts as measured by BrdU incorporation and propidium iodide (PI) flow cytometry analysis. The upper box identifies cells incorporating BrdU (S phase), the lower left box identifies G0/G1 cells and the lower right box represents G2/M cells. One of three independent experiments is reported with the percentage of cells in different cell cycle phases.

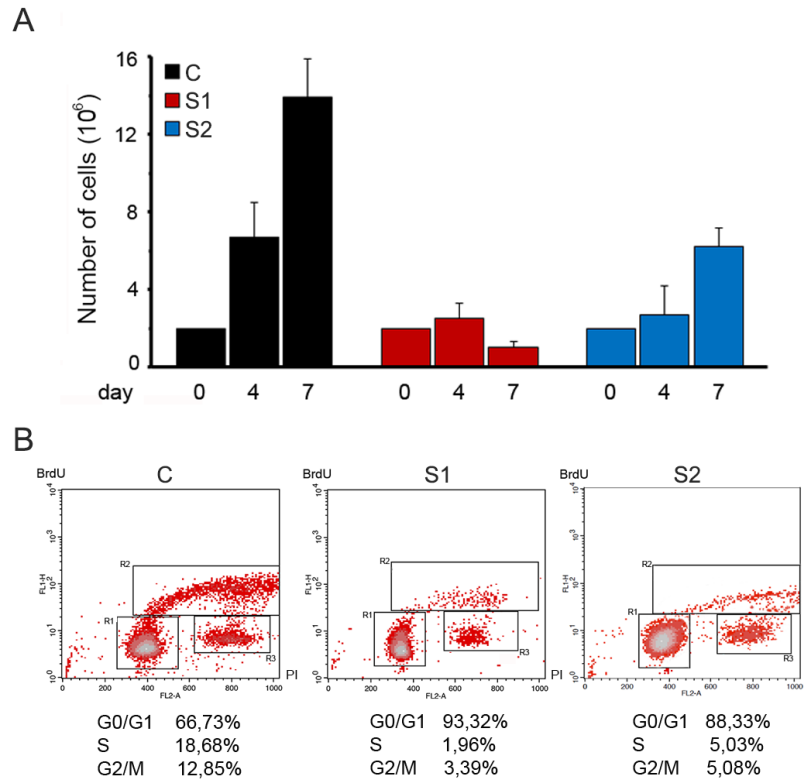
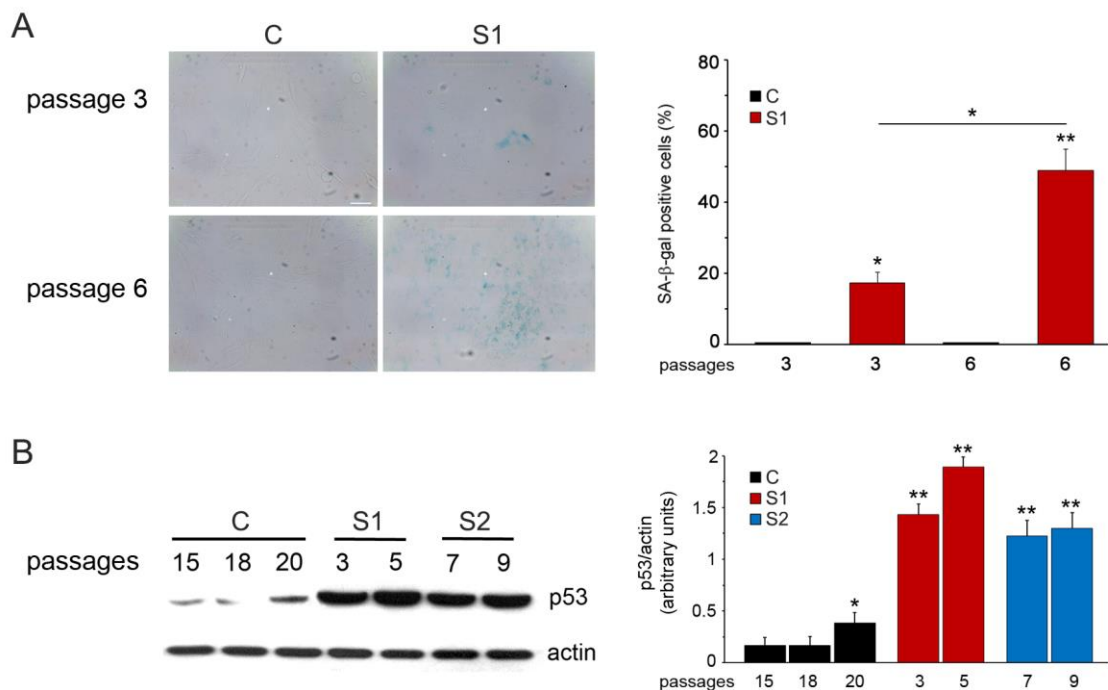


**Figure 4. Defective HISTH1E function results in altered SA- $\beta$ -gal activity and p53 expression level.** (A) Representative images (left) and quantification (right) of SA- $\beta$ -gal activity evaluated on S1 and control (C) fibroblasts at different culture passages. The significance was measured by oneway Anova with Tukey's multiple comparison test (\* $P$  < 0.01, \*\* $P$  < 0.0001). (B) Compared to control cells, enhanced TP53 protein levels were observed in S1/S2's fibroblast lysates at earlier passages. Representative blots (left) and mean  $\pm$  SD densitometry values (right) of three independent experiments are shown (\* $P$  < 0.05, \*\* $P$  < 0.002; two-tailed Student's  $t$ -test).



irregular shape. This was apparent at early passages and became more pronounced with passage of cultured cells (Figure S3). Additionally, compared to age/passage-matched control cells, fibroblasts endogenously carrying the *HIST1H1E* mutant allele were characterized by a significantly augmented SA- $\beta$ -gal activity (Figure 4A), which is an established marker of cellular senescence.<sup>46</sup> Furthermore, enhanced levels of TP53, whose amount increases during replicative senescence,<sup>47</sup> were observed at early passages (Figure 4B). These data demonstrate a direct link between aberrant *HIST1H1E* function and replicative senescence.

In premature aging disorders, replicative senescence can be caused by multiple events, including DNA double-strand breaks (DSBs), telomere dysfunction and/or accelerated shortening, as well as lamin defects.<sup>48-50</sup> To evaluate the telomere status we first performed Q-FISH analysis, which showed no difference in telomere length between control cells and fibroblasts from affected subjects (Figure S4A). Immunofluorescence analysis designed to identify  $\gamma$ H2AX foci, a marker of DSBs,<sup>51</sup> showed an increased number of positive cells and foci *per* cell among those carrying the *HIST1H1E* mutant compared to control cells (Figure S4B), indicating increased spontaneous DNA damage. ImmunoFISH analysis also documented a higher frequency of co-localization between  $\gamma$ H2AX foci and telomeres in cells from affected individuals compared to controls (Figure S4C), highlighting the presence of dysfunctional telomeres in these cells. Fibroblasts carrying the mutated *HIST1H1E* allele also showed a higher sensitivity to low doses of  $\gamma$ -ray irradiation (Figure 2E), documenting augmented susceptibility to DNA damage. These findings suggest that the proliferative arrest and senescent phenotype of cells expressing the mutant *HIST1H1E* may result, at least in part, from ineffective DNA repair and persistent activation of DNA damage response (DDR) signaling.<sup>52,53</sup> To explore this possibility, the fraction of residual DNA damage was evaluated by SCGE assay post-  $\gamma$ -ray irradiation. Kinetics data documented defective/delayed DNA repair of single and DSBs in mutant fibroblasts compared to control cells (Figure S5).

Cells carrying *LMNA* (MIM: 150330) gene mutations driving cellular senescence exhibit characteristic morphological nuclear abnormalities due to altered mechanical properties of the

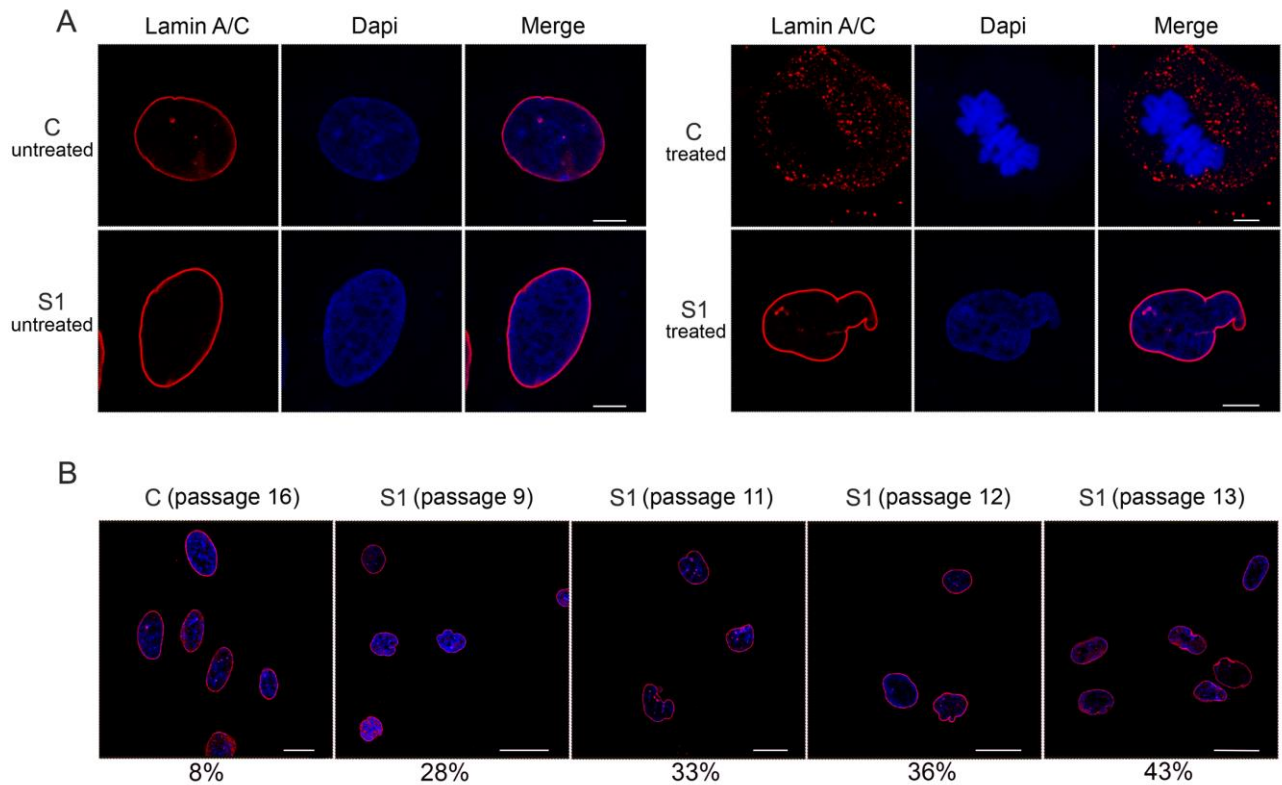


**Figure 5. Defective HISTH1E function results in aberrant nuclear morphology that is exacerbated over cell culture passages.** (A) CLSM analysis was performed in steady state (left) and synchronized (right) skin fibroblasts induced to divide after thymidine/nocodazole treatment and recovered with fresh medium. The panels show an aberrant nuclear morphology in cells from subject S1. While control cells proceed through mitosis (representative metaphases are shown), S1 fibroblasts fail to progress. Experiments were carried out at early passages (passage 3). Cells were stained using an antibody against lamin A/C (red) and DAPI (blue). Images are representative of >200 analyzed cells. Scale bars represent 7  $\mu$ m. (B) CLSM analysis was performed on S1 and control fibroblasts seeded at different culture passages. The panels show an aberrant nuclear morphology in cells from subject S1 at early passages compared to control cells, which were seeded at late passages (passage 16). Percentages refer to the number of cells with aberrant nuclear morphology. Cells were stained as above. Images are representative of > 200 analyzed cells. Scale bars represent 27  $\mu$ m.

lamina,<sup>54</sup> a network of structural filaments that interacts with chromatin to participate in chromatin remodeling and organization, and DNA replication and transcription.<sup>55-58</sup> Thus, we explored possible changes in nuclear morphology and architecture. Immunofluorescence analysis showed aberrant lamin A/C morphology in cells from affected individuals that were induced to divide after thymidine/nocodazole treatment (Figure 5A). Aberrant morphology ranged from abnormal nuclear shapes to nuclear blebbing. Of note, an increased number of aberrantly shaped nuclei in fibroblasts carrying the *HIST1H1E* frameshift was observed at early passages compared to control cells, which became more pronounced with passages ( $p < 0.0000001$ ; two-tails Fisher's exact test) (Figure 5B). This feature is reminiscent of changes in nuclear shape occurring in progeroid syndromes, and confirms the senescent phenotype associated with aberrant *HIST1H1E* function.

### ***HIST1H1E* mutations trigger nucleolar instability**

Heterochromatin plays a role in maintaining nucleolar stability and controlling rRNA synthesis,<sup>59</sup> and decreased heterochromatin levels have been associated with nucleolar instability and upregulated transcription of rRNA genes that, in turn, has been suggested to enhanced protein synthesis and contribute to overgrowth and accelerated aging.<sup>60,61</sup> Besides functioning in ribosome biogenesis, the nucleolus is involved in cell cycle control,<sup>62</sup> and linker histones have been reported to interact with multiple nucleolar proteins implicated in various nucleolar functions.<sup>63</sup> Based on these considerations, we explored whether *HIST1H1E* mutations trigger nucleolar instability. As shown, S1 fibroblasts displayed fragmentation of the nucleolus, as revealed by loss of the nucleolar marker nucleolin (Figure 6A), and showed increased amount of 18S and 28S rRNA levels (Figure 6B), further documenting the pleiotropic effect of *HIST1H1E* mutations. Notably these findings suggest that besides affecting nucleolar function, dysregulated rRNA synthesis driven by *HIST1H1E* frameshift mutations might represent the molecular event causally linked to macrosomia, a recurring feature among young children with this class of mutations.<sup>19,20</sup> This hypothesis is in line with other observations correlating tissue plasticity to ribosomal biogenesis, as

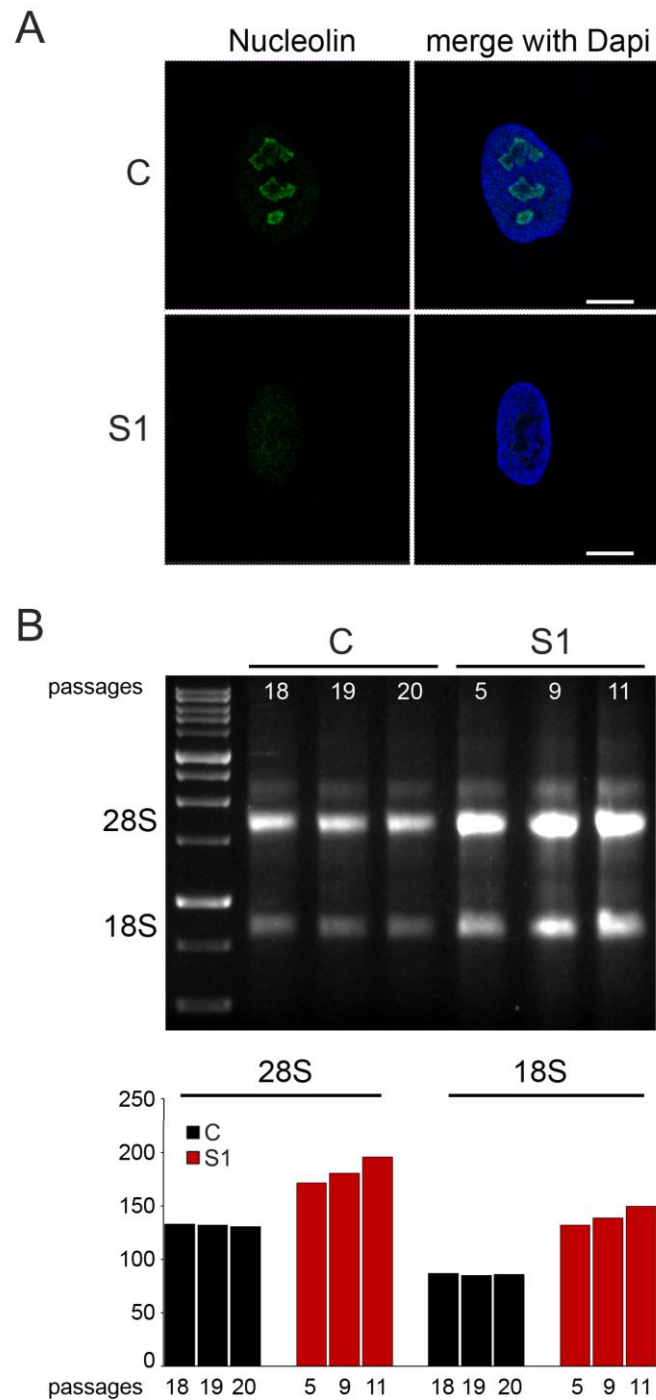


**Figure 6. Defective HIST1H1E function results in nucleolar fragmentation and increased 18S and 28S rRNA levels.** (A) CLSM observations were performed on S1 and control (C) fibroblasts. Panels show nucleolar fragmentation in S1 fibroblasts as revealed by a significant decrease in C3 clone antibody staining. Nuclei were stained with DAPI. Images are representative of > 200 analyzed cells. Scale bars represent 9  $\mu$ m. (B) Total RNA was extracted from the same amount of S1 and control (C) cells at different cellular passages. Three  $\mu$ l of total RNA was loaded for size separation on 1% agarose gel and stained with ethidium bromide. An increased amount of both 28S and 18S rRNA coding for ribosomal subunits is evident in fibroblasts from subject S1 compared to control cells.

documented for the skeletal muscle plasticity induced by seasonal acclimatization in *Cyprinus carpio*.<sup>64</sup>

**Aneuploidy is a major feature of cells bearing *HIST1H1E* frameshift**

Finally, because maximal chromatin compaction is required for proper chromosomal segregation and aneuploidy is a marker of chromosomal instability characterizing the senescent phenotype, we expected the occurrence of aneuploidy in cells expressing the disease-causing *HIST1H1E* mutants. Indeed direct count of chromosomes in metaphases revealed a remarkably high proportion of aneuploidy in early-passage fibroblasts from S1 (41.2 % of analyzed cells), which was significantly higher even when compared to late-passage control fibroblasts (18.9 % of cells) ( $P < 0.01$ ,  $\chi^2$  test).

## Discussion

Here we show that a specific class of dominantly acting frameshift mutations affecting the C-terminal tail of HIST1H1E disrupts chromatin structure and nuclear lamina organization, and drives cellular replicative senescence. By assessing the clinical records of a relatively large cohort of subjects carrying these mutations we also document that this endophenotype is mirrored by features suggestive of accelerated aging.

HIST1H1E is one of the members of the linker histone family, which function as structural components of chromatin to control the extent of DNA compaction and contribute to the regulation of gene expression and DNA replication, recombination, and repair.<sup>4,6,8,44</sup> Linker histones are encoded by multiple genes in the mammalian genomes, including paralogs characterized by a diverse expression pattern during development and having either an ubiquitous distribution or an expression restricted to specific cell types.<sup>9,65</sup> Among these, HIST1H1E has been reported to be expressed ubiquitously at a high level,<sup>65</sup> and similarly to the other replication-dependent linker histones, is synthesized during the S phase to assemble chromatin with newly replicated DNA.<sup>66</sup> As the other linker histones, HIST1H1E is relatively depleted from active promoters and other regulatory regions controlling transcription and enriched in portions of the genome carrying repressive histone marks.<sup>6</sup> Notably, previous studies provided evidence that inactivation of any of this class of histones does not significantly perturb murine development, which is compromised only when a concomitant inactivation of multiple subtypes occurs, resulting in an extensive reduction of these proteins.<sup>10,11</sup> Consistent with this functional redundancy, our data do not support haploinsufficiency as the molecular mechanism implicated in pathogenesis (see below), but point to a specific, dominantly acting effect causing a profound perturbation of multiple cellular processes directly and indirectly controlled by chromatin remodeling. Such pleiotropic effects involve genome instability, epigenetic modifications, inefficient DNA repair ability, improper chromosome compaction and segregation, nucleolar fragmentation, converging towards cellular senescence and replicative impasse.

Similarly to what is observed in progeroid disorders (*e.g.*, Hutchinson-Gilford progeria [MIM: 176670], Werner syndrome [MIM: 277700], lipodystrophy syndromes), the cellular processes affected in the disorder associated with aberrant HIST1H1E function link cellular senescence to premature aging. The clinical profile of the affected subjects with *HIST1H1E* mutations, however, differs from progeroid disorders and is quite peculiar, with a distinctive facies characterized by bitemporal narrowing, macrocephaly, prominent forehead, high anterior hairline, sparse frontotemporal hair, hypertelorism, downslanted palpebral fissures, broad nasal tip, and low-set and posteriorly rotated ears being the main features. DD/ID invariantly occurs, while overgrowth, which had been originally reported as a key feature of the disorder, was not observed in any of the subjects included in this work, at last assessment, suggesting that enhanced growth may represent a feature characterizing infancy. While the facial gestalt can help in recognition of the disorder, we noted that no pathognomonic features can be used for a definitive clinical diagnosis. In early childhood, a tentative differential diagnosis should include Pallister-Killian syndrome and mild phenotypes within the spectrum of Weaver syndrome, Werner syndrome and other progeroid disorders.

Besides documenting the multiple events contributing to cellular senescence, the present findings provide a mechanistic model for the multifaceted impact of this class of *HIST1H1E* mutations. Our data further document the specific and narrow spectrum of disease causative mutations affecting this gene. The long, lysine-rich C-terminal tail of HIST1H1E encompasses multiple regulatory residues that are substrates for cyclin-dependent kinases, with the extent of phosphorylation controlling proper compaction required for chromosome segregation, and local chromatin decondensation needed to promote DNA transcription, replication and repair. The phosphorylation of this region during the cell cycle has been theorized to contribute to the control of the chromatin state by a twofold process.<sup>3,4,12,67</sup> Partial phosphorylation is attained during interphase (G0-S phase) allowing dynamical chromatin relaxation and access to DNA.<sup>68-70</sup> On the other hand, a maximal phosphorylation is attained during mitosis (M phase), which is considered to be required for chromatin condensation and segregation of chromosomes into daughter cells during cell



division.<sup>71-75</sup> In this context, the functionally equivalent disease-causing frameshift events are the only mutations that are predicted to not significantly affect the capability of the mutant protein to retain efficient chromatin binding with concomitant loss of the regulatory sites required for modulation of higher-order chromatin architecture. Consistent with this model, the *HIST1H1E* truncating variants reported in gnomAD affect regions of the protein that do not overlap the mutational hotspot here defined, but are much more proximal to the *N*-terminus or close to the *C*-terminus (Figure S6). The former are predicted to result in truncated proteins with defective binding to chromatin and/or expected to undergo accelerated degradation, while the latter retain the regulatory serine/threonine residues and are not expected to have a dominant negative effect. The complexity by which the *C*-terminal tail controls *HIST1H1E* function, the high stability of these mutants, and their ability to bind to chromatin strongly support a dominant negative effect of these mutants. However, neomorphism/gain-of-function as alternative mechanism(s) of disease cannot be ruled out *a priori*, and dedicated studies are required to experimentally test the different models.

Taken together, the present findings provide evidence that dominantly acting functional dysregulation of a linker histone causes a complex cellular phenotype characterized by replicative senescence and results in a neurodevelopmental disorder characterized by accelerated aging.

### **Supplemental Data**

Supplemental Data include six figures and five tables.

### **Declaration of Interests**

The authors declare no competing interests.

### **Acknowledgments**

We thank the patients and their families for their participation in this study, and Serenella Venanzi (Istituto Superiore di Sanità, Rome) for technical support. This project was supported, in part, by

Fondazione Bambino Gesù (Vite Coraggiose to M.T.), the Italian Ministry of Health (Ricerca Corrente 2017 and 2018 to A.C. and M.T.), AIRC (IG21390 to G.M. and IG21614 to M.T.) and MIUR "Dipartimenti di Eccellenza" (Project D15D18000410001) to the Department of Medical Sciences, University of Turin, Italy. M.T. acknowledges CINECA for the computational resources. The Broad Center for Mendelian Genomics (UM1 HG008900) is funded by the National Human Genome Research Institute with supplemental funding provided by the National Heart, Lung, and Blood Institute under the Trans-Omics for Precision Medicine (TOPMed) program and the National Eye Institute. MHW is supported by T32GM007748. RFK and AVD are supported by grants from the ERA-NET NEURON through the Research Foundation – Flanders (FWO).

### **Web Resources**

ExAC database, <http://exac.broadinstitute.org/>;

GnomAD, <http://gnomad.broadinstitute.org/>;

Gene, <http://www.ncbi.nlm.nih.gov/gene/>;

Online Mendelian Inheritance in Man (OMIM), <http://www.omim.org/>;

Combined Annotation Dependent Depletion (CADD), <http://cadd.gs.washington.edu/>;

Database for nonsynonymous SNPs' functional predictions (dbNSFP),

<https://sites.google.com/site/jpopgen/dbNSFP>;

Gene SeT AnaLysis, <http://www.webgestalt.org/option.php>.

### **Accession Numbers**

All mutations identified in this work have been submitted to ClinVar (Submission ID: SUB5860205).

## References

- 1 Wolffe, A. (1998). *Chromatin: Structure and Function* (Academic Press, London).
- 2 Luger, K., Mäder, A.W., Richmond, R.K., Sargent, D.F., and Richmond, T.J. (1997). Crystal structure of the nucleosome core particle at 2.8 Å resolution. *Nature* 389, 251–260.
- 3 Harshman, S.W., Young, N.L., Parthun, M.R., and Freitas, M.A. (2013). H1 histones: current perspectives and challenges. *Nucleic Acids Res.* 41, 9593–9609.
- 4 Hergeth, S.P., and Schneider, R. (2015). The H1 linker histones: multifunctional proteins beyond the nucleosomal core particle. *EMBO Rep.* 16, 1439–1453.
- 5 Crane-Robinson, C. (2016). Linker histones: History and current perspectives. *Biochim. Biophys. Acta* 1859, 431–435.
- 6 Izzo, A., Kamieniarz-Gdula, K., Ramírez, F., Noureen, N., Kind, J., Manke, T., van Steensel, B., and Schneider, R. (2013). The genomic landscape of the somatic linker histone subtypes H1.1 to H1.5 in human cells. *Cell Rep.* 3, 2142–2154.
- 7 Geeven, G., Zhu, Y., Kim, B.J., Bartholdy, B.A., Yang, S.M., Macfarlan, T.S., Gifford, W.D., Pfaff, S.L., Verstegen, M.J., Pinto, H., et al. (2015). Local compartment changes and regulatory landscape alterations in histone H1-depleted cells. *Genome Biol.* 16, 289.
- 8 Bayona-Feliu, A., Casas-Lamesa, A., Reina, O., Bernués, J., and Azorín, F. (2017). Linker histone H1 prevents R-loop accumulation and genome instability in heterochromatin. *Nat. Commun.* 8, 283.
- 9 Pan, C., and Fan, Y. (2016). Role of H1 linker histones in mammalian development and stem cell differentiation. *Biochim. Biophys. Acta* 1859, 496–509.
- 10 Sirotkin, A.M., Edelman, W., Cheng, G., Klein-Szanto, A., Kucherlapati, R., and Skoultschi, A.I. (1995). Mice develop normally without the H1(0) linker histone. *Proc. Natl. Acad. Sci. USA* 92, 6434–6438.

- 11 Fan, Y., Sirotkin, A., Russell, R.G., Ayala, J., and Skoultschi, A.I. (2001). Individual somatic H1 subtypes are dispensable for mouse development even in mice lacking the H1(0) replacement subtype. *Mol. Cell Biol.* *21*, 7933–7943.
- 12 Liao, R., and Mizzen, C.A. (2016). Interphase H1 phosphorylation: Regulation and functions in chromatin. *Biochim. Biophys. Acta* *1859*, 476–485.
- 13 Kurotaki, N., Imaizumi, K., Harada, N., Masuno, M., Kondoh, T., Nagai, T., Ohashi, H., Naritomi, K., Tsukahara, M., Makita, Y., et al. (2002). Haploinsufficiency of NSD1 causes Sotos syndrome. *Nat. Genet.* *30*, 365–366.
- 14 Ng, S.B., Bigham, A.W., Buckingham, K.J., Hannibal, M.C., McMillin, M.J., Gildersleeve, H.I., Beck, A.E., Tabor, H.K., Cooper, G.M., Mefford, H.C., et al. (2010). Exome sequencing identifies MLL2 mutations as a cause of Kabuki syndrome. *Nat. Genet.* *42*, 790–793.
- 15 Qi, H.H., Sarkissian, M., Hu, G.Q., Wang, Z., Bhattacharjee, A., Gordon, D.B., Gonzales, M., Lan, F., Ongusaha, P.P., Huarte, M., et al. (2010). Histone H4K20/H3K9 demethylase PHF8 regulates zebrafish brain and craniofacial development. *Nature* *466*, 503–507.
- 16 Yuen, B.T., and Knoepfler, P.S. (2013). Histone H3.3 mutations: a variant path to cancer. *Cancer Cell* *24*, 567–574.
- 17 Maze, I., Noh, K.M., Soshnev, A.A., and Allis, C.D. (2014). Every amino acid matters: essential contributions of histone variants to mammalian development and disease. *Nat. Rev. Genet.* *15*, 259–271.
- 18 Tessadori, F., Giltay, J.C., Hurst, J.A., Massink, M.P., Duran, K., Vos, H.R., van Es, R.M., Deciphering Developmental Disorders Study, Scott, R.H., van Gassen, K.L.I., et al. (2017). Germline mutations affecting the histone H4 core cause a developmental syndrome by altering DNA damage response and cell cycle control. *Nat. Genet.* *49*, 1642–1646.
- 19 Tatton-Brown, K., Loveday, C., Yost, S., Clarke, M., Ramsay, E., Zachariou, A., Elliott, A., Wylie, H., Ardisson, A., Rittinger, O., et al. (2017). Mutations in Epigenetic Regulation

- Genes Are a Major Cause of Overgrowth with Intellectual Disability. *Am. J. Hum. Genet.* *100*, 725–736.
- 20 Takenouchi, T., Uehara, T., Kosaki, K., and Mizuno, S. (2018). Growth pattern of Rahman syndrome. *Am. J. Med. Genet. A* *176*, 712–714.
- 21 Flex, E., Niceta, M., Cecchetti, S., Thiffault, I., Au, M.G., Capuano, A., Piermarini, E., Ivanova, A.A., Francis, J.W., Chillemi, G., et al. (2016). Biallelic Mutations in TBCD, Encoding the Tubulin Folding Cofactor D, Perturb Microtubule Dynamics and Cause Early-Onset Encephalopathy. *Am. J. Hum. Genet.* *99*, 962–973.
- 22 Bauer, C.K., Calligari, P., Radio, F.C., Caputo, V., Dentici, M.L., Falah, N., High, F., Pantaleoni, F., Barresi, S., Ciolfi, A., et al. (2018). Mutations in KCNK4 that Affect Gating Cause a Recognizable Neurodevelopmental Syndrome. *Am. J. Hum. Genet.* *103*, 621–630.
- 23 Tanaka, A.J., Cho, M.T., Millan, F., Juusola, J., Retterer, K., Joshi, C., Niyazov, D., Garnica, A., Gratz, E., Deardorff, M., et al. (2015). Mutations in SPATA5 Are Associated with Microcephaly, Intellectual Disability, Seizures, and Hearing Loss. *Am. J. Hum. Genet.* *97*, 457–464.
- 24 Yang, Y., Muzny, D.M., Xia, F., Niu, Z., Person, R., Ding, Y., Ward, P., Braxton, A., Wang, M., Buhay, C., et al. (2014). Molecular findings among patients referred for clinical whole-exome sequencing. *JAMA* *312*, 1870–1879.
- 25 Vandeweyer, G., Van Laer, L., Loeys, B., Van den Bulcke, T., and Kooy, R.F. (2014). VariantDB: a flexible annotation and filtering portal for next generation sequencing data. *Genome Med.* *6*, 74.
- 26 Lek, M., Karczewski, K.J., Minikel, E.V., Samocha, K.E., Banks, E., Fennell, T., O'Donnell-Luria, A.H., Ware, J.S., Hill, A.J., Cummings, B.B., et al. (2016). Analysis of protein-coding genetic variation in 60,706 humans. *Nature* *536*, 285–291.

- 27 Retterer, K., Juusola, J., Cho, M.T., Vitazka, P., Millan, F., Gibellini, F., Vertino-Bell, A., Smaoui, N., Neidich, J., Monaghan, K.G., et al. (2016). Clinical application of whole-exome sequencing across clinical indications. *Genet. Med.* *18*, 696–704.
- 28 Andreoli, C., Leopardi, P., and Crebelli, R. (1997). Detection of DNA damage in human lymphocytes by alkaline single cell gel electrophoresis after exposure to benzene or benzene metabolites. *Mutat. Res.* *377*, 95–104.
- 29 Catanzaro, G., Besharat, Z.M., Miele, E., Chiacchiarini, M., Po, A., Carai, A., Marras, C.E., Antonelli, M., Badiali, M., Raso, A., et al. (2018). The miR-139-5p regulates proliferation of supratentorial paediatric low-grade gliomas by targeting the PI3K/AKT/mTORC1 signalling. *Neuropathol. Appl. Neurobiol.* *44*, 687–706.
- 30 Zhou, C., Cunningham, L., Marcus, A.I., Li, Y., and Kahn, R.A. (2006). Arl2 and Arl3 regulate different microtubule-dependent processes. *Mol. Biol. Cell* *17*, 2476–2487.
- 31 Cordeddu, V., Redeker, B., Stellacci, E., Jongejan, A., Fragale, A., Bradley, T.E., Anselmi, M., Ciolfi, A., Cecchetti, S., Muto, V., et al. (2014). Mutations in ZBTB20 cause Primrose syndrome. *Nat. Genet.* *46*, 815–817.
- 32 Berardinelli, F., Antoccia, A., Buonsante, R., Gerardi, S., Cherubini, R., De Nadal, V., Tanzarella, C., and Sgura, A. (2013). The role of telomere length modulation in delayed chromosome instability induced by ionizing radiation in human primary fibroblasts. *Environ. Mol. Mutagen.* *54*, 172–179.
- 33 Perner, S., Brüderlein, S., Hasel, C., Waibel, I., Holdenried, A., Ciloglu, N., Chopurian, H., Nielsen, K.V., Plesch, A., Högel, J., and Möller, P. (2003). Quantifying telomere lengths of human individual chromosome arms by centromere-calibrated fluorescence in situ hybridization and digital imaging. *Am. J. Pathol.* *163*, 1751–1756.
- 34 Morris, T.J., Butcher, L.M., Feber, A., Teschendorff, A.E., Chakravarthy, A.R., Wojdacz, T.K., and Beck, S. (2014). Champ: 450k chip analysis methylation pipeline. *Bioinformatics* *30*, 428–430.

- 35 Guarrera, S., Fiorito, G., Onland-Moret, N.C., Russo, A., Agnoli, C., Allione, A., Di Gaetano, C., Mattiello, A., Ricceri, F., Chiodini, P., et al. (2015). Gene-specific DNA methylation profiles and LINE-1 hypomethylation are associated with myocardial infarction risk. *Clin. Epigenetics* 7, 133.
- 36 Wang, J., Vasaikar, S., Shi, Z., Greer, M., and Zhang, B. (2017). WebGestalt 2017: a more comprehensive, powerful, flexible and interactive gene set enrichment analysis toolkit. *Nucleic Acids Research* 45, 130–137.
- 37 Sobreira, N., Schiettecatte, F., Valle, D., and Hamosh, A. (2015). GeneMatcher: a matching tool for connecting investigators with an interest in the same gene. *Hum. Mutat.* 36, 928–930.
- 38 Duffney, L.J., Valdez, P., Tremblay, M.W., Cao, X., Montgomery, S., McConkie-Rosell, A., and Jiang, Y.H. (2018). Epigenetics and autism spectrum disorder: A report of an autism case with mutation in H1 linker histone HIST1H1E and literature review. *Am. J. Med. Genet. B Neuropsychiatr. Genet.* 177, 426–433.
- 39 Helsmoortel, C., Vandeweyer, G., Ordoukhanian, P., Van Nieuwerburgh, F., Van der Aa, N., and Kooy, R.F. (2015). Challenges and opportunities in the investigation of unexplained intellectual disability using family-based whole-exome sequencing. *Clin. Genet.* 88, 140–148.
- 40 Kouzarides, T. (2007). Chromatin modifications and their function. *Cell* 128, 693–705.
- 41 Daujat, S., Zeissler, U., Waldmann, T., Happel, N., and Schneider, R. (2005). HP1 binds specifically to Lys26-methylated histone H1.4, whereas simultaneous Ser27 phosphorylation blocks HP1 binding. *J. Biol. Chem.* 280, 38090–38095.
- 42 Allis, C.D., and Jenuwein, T. (2016). The molecular hallmarks of epigenetic control. *Nat. Rev. Genet.* 17, 487–500.
- 43 Aref-Eshghi, E., Bend, E.G., Colaiacovo, S., Caudle, M., Chakrabarti, R., Napier, M., Brick, L., Brady, L., Carere, D.A., Levy, M.A., et al. (2019). Diagnostic Utility of Genome-wide DNA Methylation Testing in Genetically Unsolved Individuals with Suspected Hereditary Conditions. *Am. J. Hum. Genet.* 104, 685–700.

- 44 Fan, Y., Nikitina, T., Zhao, J., Fleury, T.J., Bhattacharyya, R., Bouhassira, E.E., Stein, A., Woodcock, C.L., and Skoultschi, A.I. (2005). Histone H1 depletion in mammals alters global chromatin structure but causes specific changes in gene regulation. *Cell* *123*, 1199–1212.
- 45 Criscione, S.W., Teo, Y.V., and Neretti, N. (2016). The Chromatin Landscape of Cellular Senescence. *Trends Genet.* *32*, 751–761.
- 46 López-Otín, C., Blasco, M.A., Partridge, L., Serrano, M., and Kroemer, G. (2013). The hallmarks of aging. *Cell* *153*, 1194–1217.
- 47 Kulju, K.S., and Lehman, J.M. (1995). Increased p53 protein associated with aging in human diploid fibroblasts. *Exp. Cell. Res.* *217*, 336–345.
- 48 Cau, P., Navarro, C., Harhour, K., Roll, P., Sigaudy, S., Kaspi, E., Perrin, S., De Sandre-Giovannoli, A., and Lévy, N. (2014). Nuclear matrix, nuclear envelope and premature aging syndromes in a translational research perspective. *Semin. Cell Dev. Biol.* *29*, 125–147.
- 49 Rossiello, F., Herbig, U., Longhese, M.P., Fumagalli, M., and d'Adda di Fagagna, F. (2014). Irreparable telomeric DNA damage and persistent DDR signalling as a shared causative mechanism of cellular senescence and ageing. *Curr. Opin. Genet. Dev.* *26*, 89–95.
- 50 Lidzbarsky, G., Gutman, D., Shekhidem, H.A., Sharvit, L., and Atzmon, G. (2018). Genomic Instabilities, Cellular Senescence, and Aging: In Vitro, In Vivo and Aging-Like Human Syndromes. *Front. Med.* *5*, 104.
- 51 Sedelnikova, O.A., and Bonner, W.M. (2006). GammaH2AX in cancer cells: a potential biomarker for cancer diagnostics, prediction and recurrence. *Cell Cycle* *5*, 2909–2913.
- 52 Downey, M., and Durocher, D. (2006). GammaH2AX as a checkpoint maintenance signal. *Cell Cycle* *5*, 1376–1381.
- 53 Fillingham, J., Keogh, M.C., and Krogan, N.J. (2006). GammaH2AX and its role in DNA double-strand break repair. *Biochem. Cell Biol.* *84*, 568–577.



- 54 Dahl, K.N., Scaffidi, P., Islam, M.F., Yodh, A.G., Wilson, K.L., and Misteli, T. (2006). Distinct structural and mechanical properties of the nuclear lamina in Hutchinson-Gilford progeria syndrome. *Proc. Natl. Acad. Sci. USA* *103*, 10271–10276.
- 55 Broers, J.L., Ramaekers, F.C., Bonne, G., Yaou, R.B., and Hutchison, C.J. (2006). Nuclear lamins: laminopathies and their role in premature ageing. *Physiol. Rev.* *86*, 967–1008.
- 56 Gruenbaum, Y., and Foisner, R. (2015). Lamins: nuclear intermediate filament proteins with fundamental functions in nuclear mechanics and genome regulation. *Annu. Rev. Biochem.* *84*, 131–164.
- 57 Shumaker, D.K., Dechat, T., Kohlmaier, A., Adam, S.A., Bozovsky, M.R., Erdos, M.R., Eriksson, M., Goldman, A.E., Khuon, S., Collins, F.S., et al. (2006). Mutant nuclear lamin A leads to progressive alterations of epigenetic control in premature aging. *Proc. Natl. Acad. Sci. USA* *103*, 8703–8708.
- 58 Gonzalez-Suarez, I., and Gonzalo, S. (2010). Nurturing the genome: A-type lamins preserve genomic stability. *Nucleus* *1*, 129–135.
- 59 Padeken, J., and Heun, P. (2014). Nucleolus and nuclear periphery: velcro for heterochromatin. *Curr. Opin. Cell Biol.* *28*, 54–60.
- 60 Larson, K. 1, Yan, S.J., Tsurumi, A., Liu, J., Zhou, J., Gaur, K., Guo, D., Eickbush, T.H., and Li, W.X. (2012). Heterochromatin formation promotes longevity and represses ribosomal RNA synthesis. *PLoS Genet.* *8*, e1002473.
- 61 Tsekrekou, M., Stratigi, K., and Chatzinikolaou, G. (2017). The Nucleolus: In Genome Maintenance and Repair. *Int. J. Mol. Sci.* *18*, pii: E1411.
- 62 Pederson, T. (2011). The nucleolus. *Cold Spring Harb. Perspect. Biol.* *3*, pii: a000638.
- 63 Kalashnikova, A.A., Rogge, R.A., and Hansen, J.D. (2016). Linker histone H1 and protein-protein interactions. *Biochim. Biophys. Acta* *1859*, 455–461.
- 64 Fuentes, E.N., Zuloaga, R., Valdes, J.A., Molina, A., and Alvarez, M. (2014). Skeletal muscle plasticity induced by seasonal acclimatization involves IGF1 signaling: implications in

- ribosomal biogenesis and protein synthesis. *Comp. Biochem. Physiol. B. Biochem. Mol. Biol.* 176, 48–57.
- 65 Parseghian, M.H., and Hamkalo, B.A. (2001). A compendium of the histone H1 family of somatic subtypes: an elusive cast of characters and their characteristics. *Biochem. Cell Biol.* 79, 289–304.
- 66 Happel, N., Warneboldt, J., Hänecke, K., Haller, F., and Doenecke, D. (2009). H1 subtype expression during cell proliferation and growth arrest. *Cell Cycle.* 8, 2226–2232.
- 67 Roque, A., Ponte, I., and Suau, P. (2016). Interplay between histone H1 structure and function. *Biochim. Biophys. Acta 1859*, 444–454.
- 68 Chadee, D.N., Taylor, W.R., Hurta, R.A., Allis, C.D., Wright, J.A., and Davie, J.R. (1995). Increased phosphorylation of histone H1 in mouse fibroblasts transformed with oncogenes or constitutively active mitogen-activated protein kinase. *J. Biol. Chem.* 270, 20098–20105.
- 69 Herrera, R.E., Chen, F., and Weinberg, R.A. (1996). Increased histone H1 phosphorylation and relaxed chromatin structure in Rb-deficient fibroblasts. *Proc. Natl Acad. Sci. USA* 93, 11510–11515.
- 70 Chadee, D.N., Allis, C.D., Wright, J.A., and Davie, J.R. (1997). Histone H1b phosphorylation is dependent upon ongoing transcription and replication in normal and ras-transformed mouse fibroblasts. *J. Biol. Chem.* 272, 8113–8116.
- 71 Gurley, L.R., Walters, R.A., and Tobey, R.A. (1975). Sequential phosphorylation of histone subfractions in the Chinese hamster cell cycle. *J. Biol. Chem.* 250, 3936–3944.
- 72 Hohmann, P., Tobey, R.A., and Gurley, L.R. (1976). Phosphorylation of distinct regions of fl histone. Relationship to the cell cycle. *J. Biol. Chem.* 251, 3685–3692.
- 73 Gurley, L.R., D'Anna, J.A., Barham, S.S., Deaven, L.L., and Tobey, R.A. (1978). Histone phosphorylation and chromatin structure during mitosis in Chinese hamster cells. *Eur. J. Biochem.* 84, 1–15.

- 74 Matsumoto, Y., Yasuda, H., Mita, S., Marunouchi, T., and Yamada, M. (1980). Evidence for the involvement of H1 histone phosphorylation in chromosome condensation. *Nature* 284, 181–183.
- 75 Ajiro, K., Borun, T.W., and Cohen, L.H. (1981). Phosphorylation states of different histone 1 subtypes and their relationship to chromatin functions during the HeLa S-3 cell cycle. *Biochemistry* 20, 1445–1454.